ACS APPLIED MATERIALS & INTERFACES

Research Article

www.acsami.org

Anodization of Pd in H_2SO_4 Solutions: Influence of Potential, Polarization Time, and Electrolyte Concentration

Junzhe Sun, Chi Zhang, Tianyi Kou, Junling Xu, and Zhonghua Zhang*

Key Laboratory for Liquid−Solid Structural Evolution and Processing of Materials (Ministry of Education), School of Materials Science and Engineering, Center for Advanced Energy Materials and Technology Research, Shandong University, Jingshi Road 17923, Jinan, 250061, P.R. China

Supporting Information

ABSTRACT: The anodization of Pd in H_2SO_4 solutions has been investigated by electrochemical measurements, considering the effect of the applied potential, polarization time, and electrolyte concentration. The anodization and subsequent reduction result in the formation of Pd nanostructures on the electrode surface. Compared to the bulk Pd, the anodization of Pd in H_2SO_4 solutions leads to different cyclic voltammetry (CV) behaviors including well-separated adsorption/desorption peaks in the hydrogen region and relatively larger reduction peak areas. The improvement of electrochemically active surface areas (EASAs) of the anodized Pd samples is strongly dependent upon the electrolyte concentration, and the optimum H_2SO_4 concentration is 1.0 M. Both the applied potential and polarization time have a significant influence on the anodization process of Pd. For the given electrolyte concentration, there exist desirable applied potential and polarization time to achieve greater EASAs. The EASAs of the anodized Pd obtained under the optimum polarization conditions can reach as large as 890 times compared to its geometric area. In addition, the formation mechanism of Pd nanostructures on the electrode surface has been discussed on the basis of microstructural analysis. The present findings provide a promising route to fabricate nanostructured Pd electrocatalysts with ultrahigh EASAs.

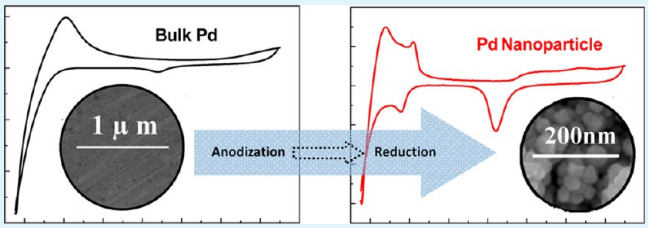

KEYWORDS: *Pd, anodization, potentiostatic polarization, cyclic voltammetry, electrochemically active surface areas (EASAs), nanostructure*

INTRODUCTION

In recent years, nanometer-sized structures have attracted increasing attention because of their potential applications in electronic, optical, and micromechanical devices. Among the approaches to the fabrication of nanostructured materials, anodization has been widely used as a simple way to produce self-organized nanostructures. This process involves the oxidation of the metal electrode and the reaction with the electrolyte, which enables the spontaneous formation of high aspect ratio nanopores on metals such as Al,[1−3] Zr,[4] Ti,[5,6] Hf,[7] W,[8] Ta,[9] and Nb.[10] Anodic porous alumina is one of typical self-organized nanostructures with a nanohole array, which can be prepared by the anodic oxidation of aluminum in an acidic electrolyte.[1,2] Anodic porous alumina with good regularity can be used as a host material to fabricate many types of nanocomposites, and it has been found that the notable regularity can be accomplished under appropriate anodizing conditions.[3] Due to its important applications in architecture and industry as well as novel regular morphology, the porous anodic film on aluminum has attracted considerable interest and the nucleation/growth mechanism has been well-studied.[2]

Moreover, other oxides such as highly ordered porous nanotubular ZrO_2 layers,[4] and self-assembled TiO_2 nanotubes[5,6] can also be obtained by the facile anodization process. Recently, it is exciting that gold, which has the highest standard redox potential among metals, has been found to form a nanoporous surface by anodization in oxalate solutions.[11] In addition, there has been some interest in the investigation of the oxide growth on Pd electrodes due to the catalytic properties of Pd and its oxidized derivatives.[12−14] To the best of our knowledge, however, little information is available on the anodization of Pd, especially on the formation of Pd nanostructures on the electrode surface.

Most recently, we have found that the anodization of Pd in a 1.0 M H_2SO_4 solution enables spontaneous formation of Pd nanoparticles, and the anodized Pd nanostructure possesses significantly larger electrochemically active surface areas (EASAs) and exhibits excellent catalytic activity toward electro-oxidation of methanol, ethanol, and formic acid in comparison to the bulk Pd.[15] In this work, we aim to investigate the effect of the applied potential (E_p), polarization time (t_p) and electrolyte concentration (c) on the anodization process of Pd in aqueous H_2SO_4 solutions. Meanwhile, the anodized Pd with relatively larger EASAs can be obtained by the optimization of the anodization parameters (E_p, t_p, and c). In

Received: August 17, 2012
Accepted: October 31, 2012
Published: October 31, 2012

addition, the formation mechanism of the Pd nanostructure on the electrode surface has also been discussed.

EXPERIMENTAL SECTION

Prior to electrochemical anodization, Pd foils (0.1 mm thickness, 99.9 wt.% purity) were rinsed with acetone, alcohol and ultrapurified water (18.2 MΩ). Anodization experiments were performed in a standard three-electrode cell with a plate-like Pt counter electrode using a LK 2005A Potentiostat. The samples were sealed by epoxy resin to expose a geometric area of 0.10 cm^2 and used as the working electrode. The H_2SO_4 electrolytes with different concentrations were prepared from concentrated H_2SO_4 and ultrapurified water. The saturated calomel electrode (SCE) or Hg/Hg_2SO_4 (MSE) were used as the reference electrode.

The cyclic voltammetry (CV) curves of the Pd electrode were first recorded in various H_2SO_4 solutions with a SCE reference electrode in order to preactivate the Pd electrode and achieve reproducible polarization curves. The applied potentials (E_p) were determined according to the positive-going linear sweep voltammetry (LSV) curves in various H_2SO_4 solutions using the MSE reference electrode. Anodization experiments of Pd were conducted under potentiostatic conditions (E_p = const.) in the H_2SO_4 solutions with various concentrations (c = 0.1, 0.5, 1.0, 2.0, 3.0, 4.0, and 5.0 M) for different polarization times (ranging from 15 s to 120 min). Then the anodized samples were reduced during CV scans between −0.25 and 1.1 V (vs SCE) for 20 cycles in the corresponding H_2SO_4 solutions. During all potential sweep processes, the scan rate of potential was 50 mV s^{-1}. After the anodization and CV reduction, Pd nanostructures formed on the surface of the Pd electrode. For simplicity, the as-obtained samples were denoted as the anodized Pd. In order to evaluate the EASAs of the anodized Pd samples, CV measurements were also performed between −0.25 and 1.1 V (vs SCE) for 20 cycles in the 1.0 M H_2SO_4 solution with SCE as the reference electrode. The EASAs of the anodized Pd electrodes were calculated by integration of the cathodic peaks (as shown in Figure S1 in the Supporting Information) corresponding to reduction of Pd oxide monolayer formed in the previous anodic scan,[16] accepting a charge density of 424 μC cm^{-2} as the charge necessary to form a monolayer of electro-adsorbed O allowing for the double-layer charging.[17,18] The interpretation for the evaluation method of the EASA was detailedly presented in Figure S1 (Supporting Information). In addition, the electrode potentials were sometimes transformed with respect to reversible hydrogen electrode (RHE) if necessary ($E_{RHE} = E_{SCE} + 0.242$ V, $E_{RHE} = E_{MSE} + 0.652$ V). Microstructural characterization and analysis of the anodized Pd samples were carried out using an X-ray diffractometer (XRD, Rigaku D/max-rB) with Cu Kα radiation and a scanning electron microscope (SEM, FEI QUANTA FEG 250) equipped with an energy-dispersive X-ray (EDX, Oxford X-MAX50) analyzer.

RESULTS AND DISCUSSION

Effect of H_2SO_4 Concentrations on Anodization of Pd.

Figure 1a shows the typical CV curves of the bulk Pd electrodes before anodization in the H_2SO_4 solutions with concentrations of 0.1, 0.5, 1.0, 2.0, 3.0, 4.0, and 5.0 M, which are similar to other previously reported profiles of Pd.[19,20] It can be seen that in the potential range of −0.25−0.2 V (vs SCE) (Figure 1a), the bulk Pd electrodes before anodization do not display well-separated processes of hydrogen adsorption, desorption and evolution. In the cathodic scan the current starts to increase rapidly at about 0 V (vs SCE), and the peaks in the anodic scan correspond to the oxidation of absorbed hydrogen. Moreover, the hydrogen region area becomes larger with increasing electrolyte concentrations. On the other hand, the cathodic curves of the bulk Pd electrodes present a reduction peak of previous Pd surface oxide at ~0.5 V (vs SCE) in various H_2SO_4 concentrations, which can be seen clearly in the enlarged view (inset of Figure 1a). It can be seen that the reduction peak

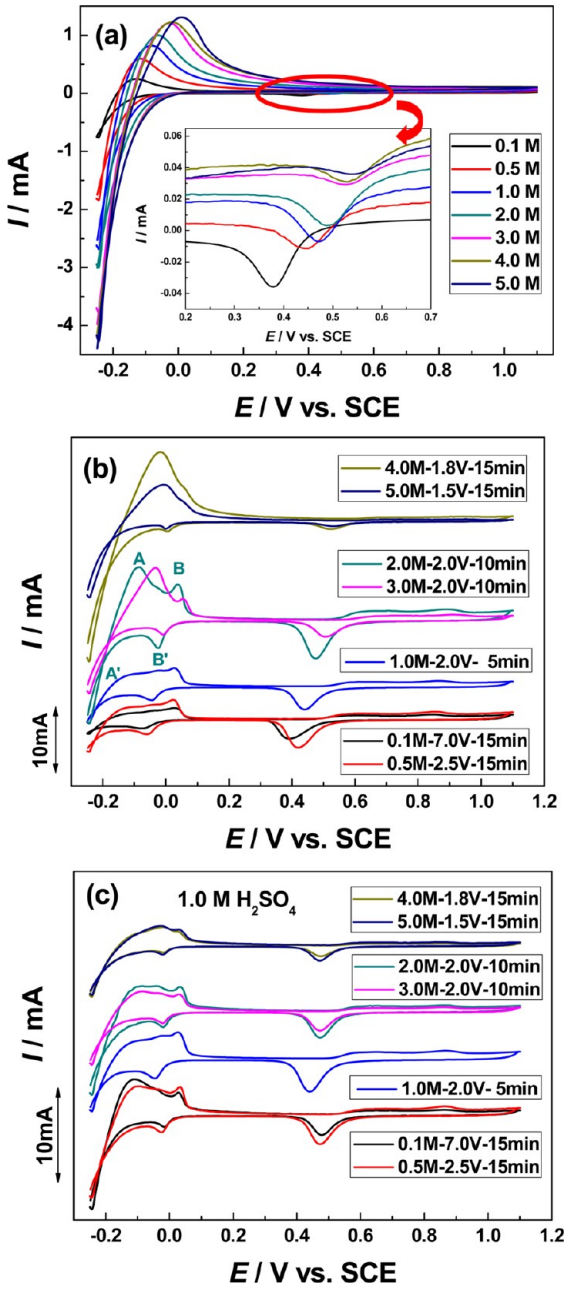

Figure 1. CVs for (a) the bulk Pd electrodes and (b) the anodized Pd samples obtained under the given potentials (vs MSE) and polarization times in the corresponding H_2SO_4 solutions with various concentrations, and (c) the anodized Pd samples (obtained under different conditions) in the 1.0 M H_2SO_4 solution.

potentials (E_r) slightly shift to the more positive positions with increasing H_2SO_4 concentrations, implying that the Pd surface oxide has been reduced more easily in higher H_2SO_4 concentrations in the negative scan, and the corresponding E_r (vs SCE) values are listed in Table S1 in the Supporting Information.

Figure 1b displays the representative CV curves of the Pd electrodes after anodization/CV reduction at the given potentials in the 0.1, 0.5, 1.0, 2.0, 3.0, 4.0, and 5.0 M H_2SO_4 solutions. Comparing with the corresponding CVs of the bulk Pd electrodes before anodization (Figure 1a), it can be seen that the anodized Pd electrodes exhibit distinct behaviors (Figure 1b). As shown in Figure 1b, taking the CV for the

dx.doi.org/10.1021/am301685f | ACS Appl. Mater. Interfaces 2012, 4, 6038−6045

anodized Pd obtained at 2.0 V (vs MSE) for 10 min in the 2.0 M H_2SO_4 solution as an example, two obvious pairs of distinct current peaks in the hydrogen region (A and A′, B and B′) appear in the CV profiles. The relative large pair of current peaks at a more negative potential (A and A′) are related to bulk (absorbed) H-atoms, while the small current peaks (B and B′) at a more positive potential are associated with the hydrogen underpotential deposition (H-UPD) adsorbed H-atoms.[21] On one hand, for the cathodic scan one minor peak appears at approximately −0.05 V (vs SCE) (Figure 1b) on each of the CV curves in different H_2SO_4 concentrations, indicating that the hydrogen atoms have started to be adsorbed on the Pd surface in the H-UPD range. It is well-known that hydrogen is strongly adsorbed on the Pd surface and can be absorbed to a large extent into the Pd lattice. The adsorbed hydrogen atoms immediately become absorbed (H_{abs}) in the H-UPD range, and the UPD H adsorption and absorption may occur concurrently.[22,23] With further negative-going of the applied potential, the current increases rapidly because of the H overpotential deposition (OPD). And some H_{OPD} atoms also become absorbed, accompanied by a large amount of H_2 generation.[24] On the other hand, with the change of the electrolyte concentrations the hydrogen regions in the anodic scan have a slight difference between them. When the concentrations are below 1.0 M, an obvious peak appears at ~0.05 V (vs SCE) in the hydrogen region in the positive scan, while another peak between −0.1 and 0 V (vs SCE) occurs in the 2.0 and 3.0 M H_2SO_4 solutions. In addition, with further increasing electrolyte concentrations (4.0 and 5.0 M), the main peak at the more negative potential has nearly covered the minor peak. It is speculated that in the positive-going scans, the first peak at the lower potential is ascribed to the desorption of H from the bulk Pd, while the second peak at the more positive potential is related to the UPD adsorbed H atoms, which need a higher energy to release these adsorbed H atoms. Thus it is reasonable to assume that the peaks in the positive-going scans could be related to different energetic states of H that undergoes desorption, which is affected by the concentrations of H^+ in the H_2SO_4 solutions.

Moreover, various Pd nanostructured materials with large specific surface areas, such as ultrathin Pd film,[25] Pd nanoparticles,[26] and nanoporous Pd[27] have been found to exhibit the similar CV behaviors. According to the behavior in the hydrogen region, it is reasonable to assume that Pd nanostructures form on the surface of the anodized Pd samples. Moreover, the oxide film has been gradually formed on Pd at the beginning of broad oxidation current peak in the positive scan and then it can be reduced in the corresponding reduction peak during the negative-going transient.[28,29] It has been reported that a Pd electrode covered with a layer of PdO has a redox potential of 0.891 V (vs RHE), whereas the redox potential for the same electrode covered with PdO_2 (on top of PdO) is 1.491 V (vs RHE) (eqs 1 and 2) .[30]

$$PdO + 2H^+ + 2e^- \rightarrow Pd + H_2O$$
$$E_{Pd^{2+}/Pd} = 0.891V \text{ (vs. RHE)} \quad (1)$$

$$PdO_2 + 4H^+ + 4e^- \rightarrow Pd + 2H_2O$$
$$E_{Pd^{4+}/Pd} = 1.491V \text{ (vs. RHE)} \quad (2)$$

Furthermore, because a simultaneous transfer of two electrons is unlikely, the process of oxygen desorption is assumed to occur via two consecutive steps, with the intermediate formation of the one-electron transfer product PdOH as proposed by Bagotzky and Tarasevich.[31] Nevertheless it has been proposed that the formation of PdOH is the first step of the electro-oxidation of Pd in both acidic and basic electrolytes,[32,33] it is reasonable to assume that PdOH is not a surface species formed in the electro-oxidation of Pd in acidic electrolytes.[34]

In addition, it is obvious that the reduction peak area of the anodized Pd electrode is significantly larger than that of the bulk one (Figure 1a, b), indicating the higher EASAs of the anodized Pd samples. In order to evaluate the EASAs of the anodized Pd, a set of CVs were recorded in the 1.0 M H_2SO_4 solutions, and Figure 1c shows the representative CV curves of the anodized Pd samples obtained under various conditions. Well-separated adsorption−desorption peaks can be clearly observed in the hydrogen region for all the anodized Pd samples (Figure 1c). Similarly, the obvious reduction peaks of Pd can also be seen in the negative scan. In addition, all the EASAs of the anodized samples were evaluated according to the method interpreted in Figure S1 in the Supporting Information.

Figure 2a shows the positive-going LSV curves of the bulk Pd electrodes in the 0.1, 0.5, 1.0, 2.0, 3.0, 4.0, and 5.0 M H_2SO_4 solutions. It is clear that there exist a critical potential (E_c) on all the LSV curves, as marked by a downward arrow in Figure 2a. Moreover, the electrolyte concentration has no obvious

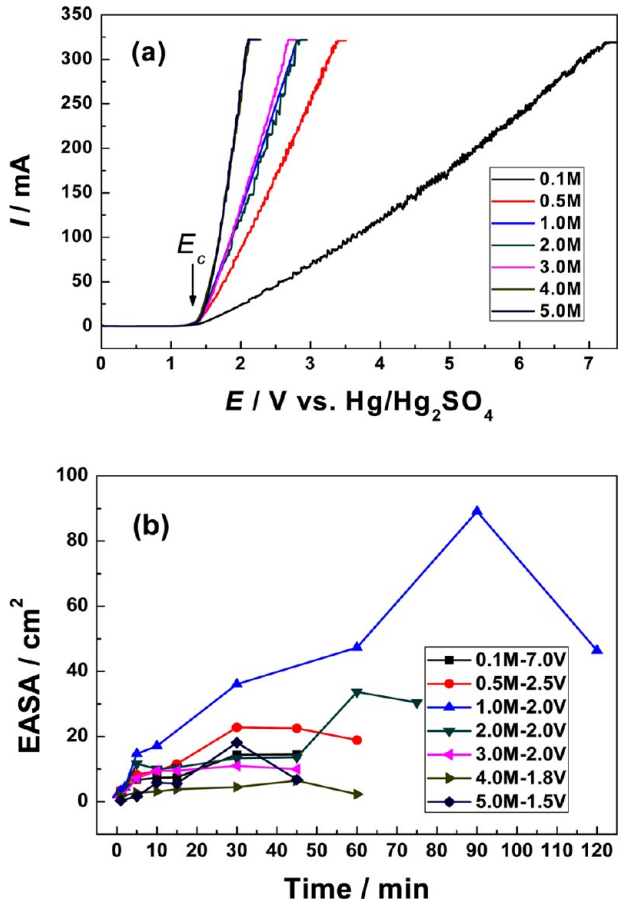

Figure 2. (a) Positive-going LSV curves of the bulk Pd electrodes in the H_2SO_4 solutions with various concentrations, and (b) plot of EASAs vs polarization times for the anodized Pd samples obtained in the various H_2SO_4 solutions at different applied potentials (vs MSE).

dx.doi.org/10.1021/am301685f | ACS Appl. Mater. Interfaces 2012, 4, 6038−6045

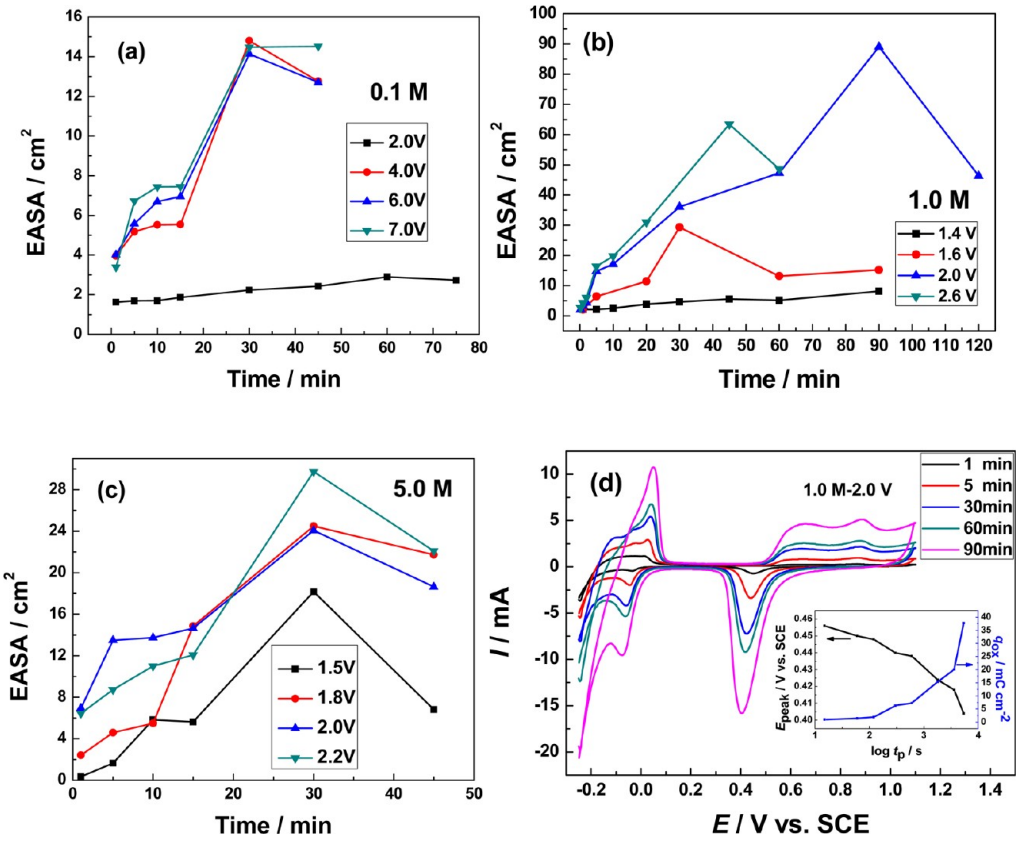

Figure 3. Plot of EASAs vs polarization times for the anodized Pd electrodes obtained in the (a) 0.1 M,(b) 1.0 M and (c) 5.0 M H_2SO_4 solutions at different applied potentials (vs MSE). (d) CVs for the anodized Pd electrodes obtained under different conditions in the 1.0 M H_2SO_4 solution. (The inset demonstrates the charge density, q_{ox}, and the peak potential, E_{peak}, as a function of log t_p.).

influence on the critical potential, which is located at ~1.3 V (vs MSE). Coincidently, the critical potential also exists in dealloying, which is defined as the onset of the selective dissolution in alloy corrosion and indicates the transition from the passive-like behavior to selective dissolution on the alloy polarization curves.[35,36] Similarly, as to the bulk Pd, below E_c all the LSV curves almost overlap and the currents keep constant (close to zero) with increasing potential, which exhibits the similar behavior of the passive-like state to dealloying. However, above E_c, the currents rapidly increase with increasing potential, and the electrolyte concentration has a significant influence on the slopes of the LSV curves (Figure 2a). On the whole, the slopes of the LSV curves obviously increase with increasing electrolyte concentration. With further observation this enhancement tendency is more obvious in the low concentration range of the H_2SO_4 solutions (below 1.0 M). Moreover, the LSV curves are almost identical in the H_2SO_4 solutions with concentrations of 1.0, 2.0, and 3.0 M. A similar scenario also occurs in the 4.0 and 5.0 M H_2SO_4 solutions. It can be deduced that, the amount of H^+ concentration in the solution has a profound effect on the current−potential behavior when the H_2SO_4 concentration is low. Although with the further increase in the concentrations to a certain value, the currents rapidly increase with increasing potential and the slopes of the LSV curves almost remain unchanged among these H_2SO_4 solutions with high concentrations. It can be speculated that the amount of H^+ concentration is enough to supply the reaction when the H_2SO_4 concentration is above 1.0 M, and thus the concentration of H_2SO_4 has a minor influence on the current−potential behavior. In addition, to achieve an appreciable oxidation current (or current density), a higher potential is necessary for a lower electrolyte concentration. According to these LSV curves, the applied potentials E_p were determined and the corresponding E_p (vs MSE) values are also listed in Table S1 (Supporting Information).

Figure 2b shows EASAs vs polarization times for the anodized Pd electrodes obtained in the various H_2SO_4 solutions at different applied potentials. For each electrolyte concentration, the typical results are presented in Figure 2b at an appropriate applied potential. When the H_2SO_4 concentration is low (0.1 M), the EASAs can be improved at relatively high potential (7.0 V (vs MSE)). With increasing H_2SO_4 concentration to 0.5 M, the EASAs have been further increased even at the applied potential of 2.5 V (vs MSE). It can be found that the EASAs of the anodized Pd samples obtained in the 1.0 M H_2SO_4 solution are much higher than those obtained in other H_2SO_4 solutions. The EASA can reach ~89 cm^2 at the applied potential of 2.0 V (vs MSE), which is ~890 times that the geometric area (0.1 cm^2) of the bulk Pd electrode. When the anodization of Pd was performed in the H_2SO_4 solutions with high concentrations of above 2.0 M, the EASAs of the anodized samples have limited improvement, compared to the bulk Pd electrode. Hence, the improvement of EASAs of the anodized Pd samples is crucially dependent on the electrolyte concentration, and the optimum H_2SO_4 concentration is 1.0 M.

According to the roughness factor ($r^w = A_{real}/A_{geom}$) proposed by Wenzel,[37] r^w values of the anodized Pd electrodes were determined and also listed in Table S1 (Supporting Information). On the whole, the anodized Pd electrodes have much larger r^w than that ($r^w \approx 2.6$[15]) of the bulk Pd electrode,

dx.doi.org/10.1021/am301685f | ACS Appl. Mater. Interfaces 2012, 4, 6038−6045

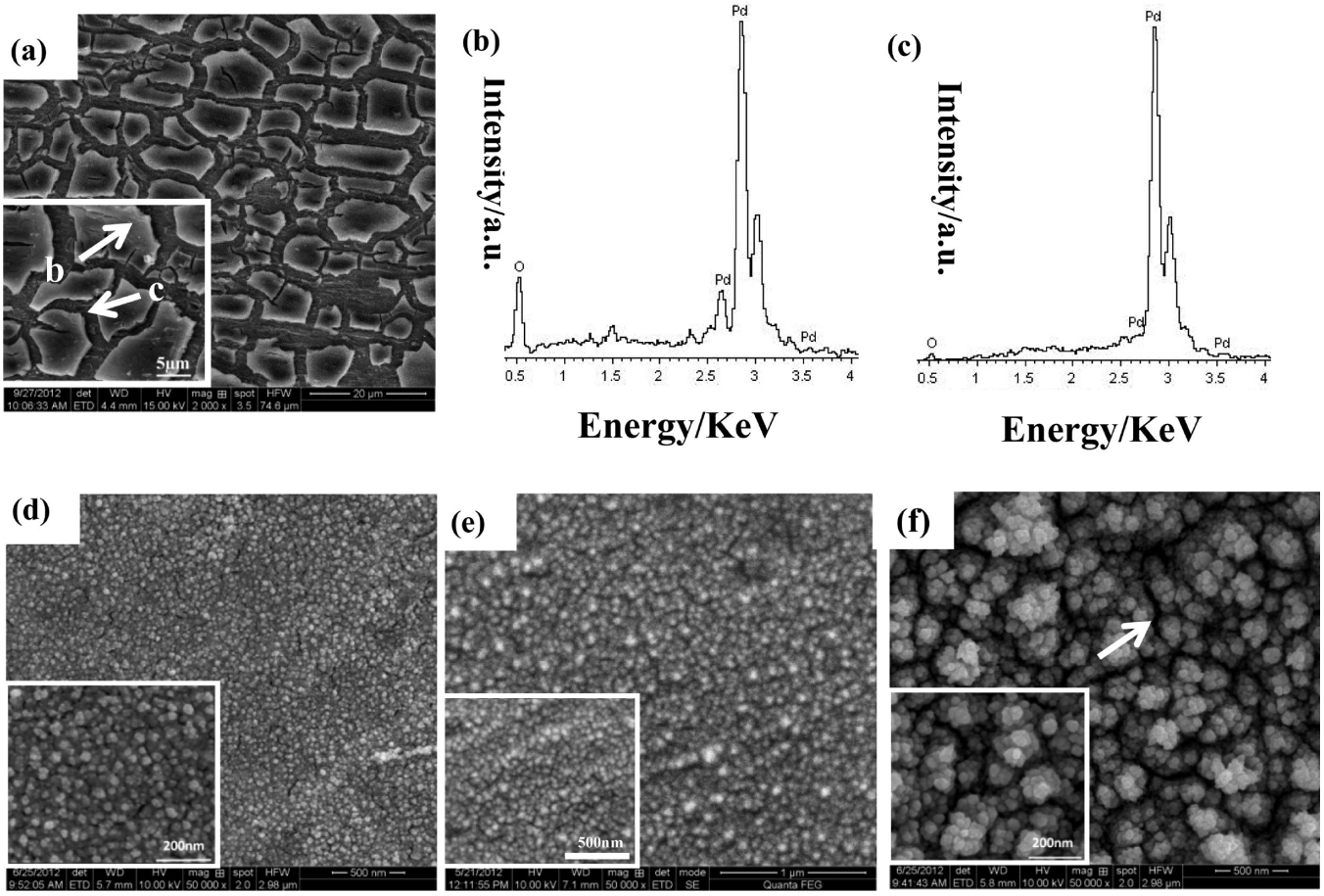

Figure 4. (a) SEM micrograph of the Pd electrode anodized at 2.0 V (vs MSE) in the 1.0 M H_2SO_4 solution for 60 min, (b, c) corresponding EDX spectra of the selected area (marked by arrows in the inset of a), (d–f) SEM micrographs of the anodized Pd samples after reduction obtained at 2.0 V (vs MSE) in the 1.0 M H_2SO_4 solution for 2, 10, and 90 min, respectively. The insets are the corresponding enlarged views.

suggesting that the anodization process enables the formation of Pd nanostructures on the surface, which contributes to the larger reduction peak areas on the CV curves and is beneficial to the electrocatalytic activity.[15] It has been reported that some changes in the surface morphology of Pd oxides can be observed during repetitive oxide formation and reduction cycles due to the rearrangement of surface atoms (quasirecrystallization), which modifies the electrode's surface roughness.[38−40] Moreover, the changes in surface roughness could result in either an increase or a decrease of the surface area depending on the applied potential.[38,39,41] The increase in the electrode's roughness can be ascribed to the repetitive formation and reduction of thick Pd oxide layers,[42] rather than the redeposition of previously dissolved Pd cations.[43] Similar surface roughness changes were reported for Pt electrodes[44] and the mechanism proposed for Pd is in agreement with that for Pt.[42] Here, the improvement in roughness of the anodized Pd electrodes is mainly due to the formation of Pd nanostructures, which will be clarified in the following section.

Effect of Applied Potential and Polarization Time on Anodization of Pd. To further investigate the influence of the applied potential and polarization time, we selected four potentials in each of the 0.1, 1.0, and 5.0 M H_2SO_4 solutions. Figure 3a–c displays the EASAs vs polarization times for the anodized Pd electrodes in the 0.1, 1.0, and 5.0 M H_2SO_4 solutions at different applied potentials, respectively. As a whole, the EASAs of the anodized Pd samples become larger when increasing the applied potential (E_p vs MSE) in the same H_2SO_4 solution. When the E_p increases to a certain value, however, the EASAs can be hardly further improved. Hence, the applied potential has an appropriate range to obtain larger EASAs in the given H_2SO_4 concentration. It can be found that the optimum applied potential is approximately 2.0 V (vs MSE) in the 1.0 M H_2SO_4 solution (Figure 3b).

On the basis of the careful observation of the EASAs vs polarization time curves in Figure 3, it can be found that at the given applied potential, almost all the EASAs exhibit the same variation trend with polarization time in the same H_2SO_4 solution. The EASAs first increase rapidly with extending the polarization time, and then keep a slow increasing trend with further prolonging the polarization time. The EASAs even decrease after the given polarization time (Figure 3a–c). In fact, the decrease in EASAs is mainly caused by the shedding of the surface layer of the Pd electrodes during the anodization process. We have observed the shedding of the surface layer after long polarization times. The reason for the shedding will be discussed in the mechanism section. The present results demonstrate that there exists a proper polarization time for the anodization of Pd at the given applied potential in the given H_2SO_4 solution.

Figure 3d shows the representative CVs of the anodized Pd electrodes obtained at 2.0 V (vs MSE) in the 1.0 M H_2SO_4 solution for different polarization times. Other CVs of the anodized Pd electrodes obtained under different conditions are

dx.doi.org/10.1021/am301685f | ACS Appl. Mater. Interfaces 2012, 4, 6038−6045

shown in Figures S2−S5 in the Supporting Information. According to these CVs, the cathodic peaks corresponding to the reduction of PdO to Pd were integrated and the EASAs of the anodized Pd samples were calculated. As shown in Figure 3d, the adsorption−desorption peaks become more pronounced in the hydrogen region with increasing polarization time. Similar scenarios can also be observed for the broad oxidation peaks of Pd in the positive scan and reduction peaks in the negative scan. In addition, the charge density of the oxide layer, q_{ox}, was also evaluated. In the inset of Figure 3d, two curves which relate the reduction peak potential (E_{peak}) and the oxide charge density (q_{ox}) to the polarization time (t_p) are presented. It can be found that the extension of t_p not only results in greater q_{ox}, but also causes a shift of E_{peak} toward more negative positions, which has been observed in the literature.[45] With prolonging t_p, thicker oxide films form and thus the EASAs increase, resulting in the increase of q_{ox}.

Microstructure of the Anodized Pd Electrodes. To make clear the anodization process and the microstructural evolution of the anodized Pd, we performed SEM observation and EDX analysis for the anodized Pd electrode before and after CV reduction. Figure 4a shows the SEM image of the Pd electrode anodized at 2.0 V (vs MSE) in the 1.0 M H_2SO_4 solution for 60 min, and corresponding EDX spectra of the selected areas are shown in Figure 4b, c. Figure 4d−f shows the SEM images of the anodized Pd samples after reduction obtained at 2.0 V (vs MSE) in the 1.0 M H_2SO_4 solution for 2, 10, and 90 min, respectively. From Figure 4a, it can be seen that a large amount of cracks appear on the Pd surface during the oxide formation process and the cracks separate the electrode surface into splintery regions. The EDX results show that the surface of Pd has been fully oxided (Figure 4b), whereas the ravine of the cracks was going to be oxided with the evidence of low content of oxygen (Figure 4c). The chemical composition of the splintery regions was determined to be 48 at % Pd and 52 at % O (Figure 4b). The EDX analysis demonstrates that the atomic ratio of Pd/O is close to 1:1 in the splintery surface regions, indicating the formation of the PdO oxide. At the same time, the appearance of the cracks is beneficial to the further oxidation of deeper Pd atoms. From Figure 4d−f, it can be clearly seen that the anodized Pd samples after reduction are composed of a large amount of nanoparticles. Together with the higher magnification images shown as insets in Figure 4d−f, the length scale of these Pd nanoparticles is approximately 50 nm. It is reasonable to think that these nanoparticles contribute to the excellent catalytic activity toward electro-oxidation of methanol, ethanol, and formic acid due to their large specific surface areas and more active sites.[15] Although the size of the nanoparticles has no obvious change with increasing polarization time, the morphology of the anodized Pd differs a lot among these three samples. A large amount of Pd nanoparticles distribute uniformly on the surface of the anodized Pd with the polarization time of 2 and 10 min (Figure 4d, e). When further prolonging the polarization time to 90 min, Pd nanoparticles congregate to form islands in the anodized Pd sample (Figure 4f). Moreover, microcracks appear between these islands, and one is highlighted by an arrow in Figure 4f. During the anodization process, the Pd atoms on the surface are first anodized. With increasing polarization time, the inner Pd atoms will participate in the reaction, and the anodization goes deep into the Pd electrode. This can be further verified in Figure 4f.

Mechanism and Kinetics of Anodization on Pd. Figure 5 shows the XRD patterns of the Pd electrode anodized at 1.6 V (vs MSE) for 60 min in the 1.0 M H_2SO_4 solution before and after CV reduction. According to the XRD results, it is clear that the anodized Pd electrode (before CV reduction) is mainly composed of two phases: face centered cubic (f.c.c.) Pd and PdO (Figure 5a). The anodized oxide film on Pd is confirmed to be PdO. This is in accordance with the above EDX results (Figure 4b). Moreover, the significant broadening of diffraction peaks of PdO indicates its small grain sizes. After the CV reduction, PdO has been reduced to Pd, which can be confirmed in Figure 5b. Grdeń and co-workers have found that oxidized Pd has been formed involving the process of anion and cation adsorption/desorption, interaction of water molecules with the electrode surface, formation of surface oxides, and electrodissolution.[29] Moreover, the formation of oxide layers on Pd is also assumed to occur in a stepwise fashion. With increasing anodized potential, a monolayer of PdOH is produced that can be changed electrochemically into a more stable layer of PdO. At the same time, this relatively slow transformation process also includes surface reconstruction as the initial step for the diffusion of oxygen into the bulk metal.[27] During the Pd oxidation formation process, the stress caused by the crystal lattice expansion/contraction (because of the great difference in lattice between Pd and PdO) has generated together with a large amount of gas, which could separate the oxide film from the matrix. Thus obvious shedding of the oxide film on Pd can be seen during the anodization process after long polarization times, leading to the decrease of EASAs (Figure 3a−c). Similar phenomena can also be found in other CVs shown in Figures S2−S5 in the Supporting Information. In addition, the repetitive oxide formation and reduction process

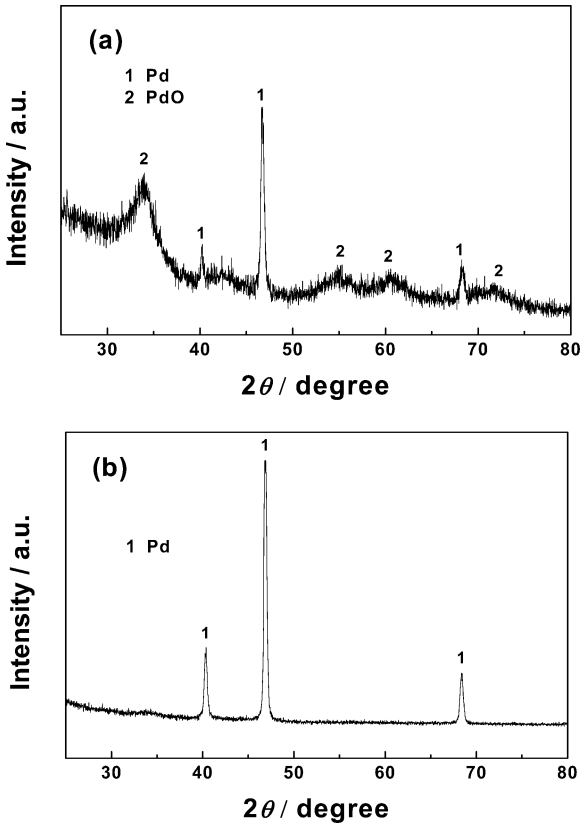

Figure 5. XRD patterns of the Pd electrode (a) anodized at 1.6 V (vs MSE) for 60 min in the 1.0 M H_2SO_4 solution and (b) after CV reduction.

dx.doi.org/10.1021/am301685f | ACS Appl. Mater. Interfaces 2012, 4, 6038−6045

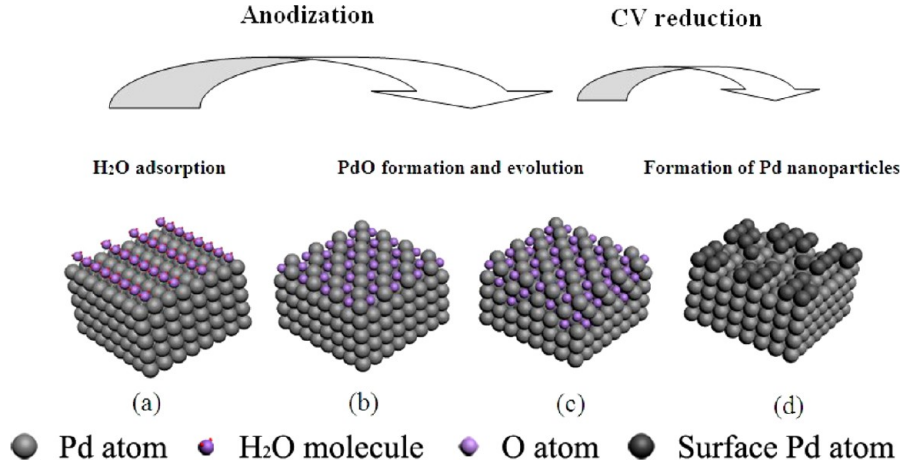

Figure 6. Schematic illustration showing the formation process of Pd nanoparticles through the anodization and CV reduction.

enables the rearrangement of atoms in the surface region (quasirecrystallization), which finally results in the spontaneous formation of Pd nanoparticles.

The above results demonstrate that Pd nanoparticles form on the Pd electrode after the CV reduction (Figures 4 and 5). Figure 6 illustrates the formation process of nanoparticles on Pd. The formation mechanism of Pd nanoparticles can be rationalized as follows: (1) H_2O molecules first adsorb on the Pd electrode surface (Figure 6a), (2) the intermediate PdOH thus forms by one-electron transfer and subsequently transforms to PdO on the electrode surface (Figure 6b), (3) the sublayer Pd atoms take part in the reaction with extending the polarization times (Figure 6c), (4) Pd atoms rearrange to form Pd nanoparticles during the reduction of PdO to Pd (Figure 6d). It should be noted that Figure 6 just presents a proposal of a mechanism that results in nanostructures on Pd. At the present time, there are no real-time images (e.g., scanning tunnel microscopy, STM) that would confirm that the proposed mechanism is correct. The underlying mechanism will be further probed in the following work.

Generally speaking, the growth of thin surface oxides on noble-metal electrodes is logarithmic or inverse-logarithmic in oxidation time.[40,46] To analyze the growth kinetics and mechanism, it is customary to present q_{ox} or $1/q_{ox}$ versus t_p on a logarithmic scale.[47,48] On the basis of the CV curves, we can examine q_{ox} or $1/q_{ox}$ versus log t_p for the entire range of electrolyte concentrations. When we plot $1/q_{ox}$ versus log t_p (shown in Figure S6 in the Supporting Information), the relation is approximately linear, implying the inverse-logarithmic growth mechanism. This means that the oxide growth is limited by the escape of the metal cation from the metal into the oxide at the inner metal/oxide interface, and the mechanism has been proposed and discussed by Cabrera and Mott in detail.[49]

CONCLUSIONS

(1) The anodization process on Pd under different conditions results in different CV behaviors in H_2SO_4 solutions compared to the bulk Pd, including separated adsorption/desorption peaks in hydrogen region and relatively larger reduction peak areas.

(2) The improvement of EASAs of the anodized Pd samples is dependent on the electrolyte concentration, and the optimum H_2SO_4 concentration is 1.0 M.

(3) Both the applied potential and polarization time have a significant influence on the anodization process of Pd. As a whole, the EASAs of the anodized Pd markedly increase with increasing applied potential at the given electrolyte concentration, and the applied potential has an appropriate range to obtain larger EASAs. At the given applied potential and electrolyte concentration, the EASAs increase first to the maximum value and then decrease with increasing polarization time, which is due to the shedding of the anodized film on Pd.

(4) Considering the combination effect of the applied potential, polarization time, and electrolyte concentration, the optimized anodization condition was determined to be at 2.0 V (vs MSE) in the 1.0 M H_2SO_4 solution for 90 min. The EASAs of the anodized Pd obtained under these conditions can reach as large as 890 times compared to its geometric area.

(5) The formation of PdO layers on Pd is assumed to occur in a stepwise stage under potentiostatic conditions in the H_2SO_4 solution, and the growth is controlled by the inverse-logarithmic mechanism. Moreover, Pd nanoparticles can spontaneously form by the combination of anodization with subsequent reduction in H_2SO_4 solutions, which provides a promising route to fabricate nanostructured Pd catalysts with ultrahigh EASAs.

ASSOCIATED CONTENT

Supporting Information

Summary of the parameters of the anodized Pd samples obtained under different conditions; the interpretation for the evaluation method of the EASA; CV curves recorded in the 1.0 M H_2SO_4 solutions for the anodized Pd obtained under different conditions in the 0.1, 0.5, 1.0, 2.0, 3.0, 4.0, and 5.0 M H_2SO_4 solutions; and the plot of $1/q_{ox}$ vs log t_p for the anodized Pd. This material is available free of charge via the Internet at http://pubs.acs.org/.

AUTHOR INFORMATION

Corresponding Author

*Email: zh_zhang@sdu.edu.cn.

Notes

The authors declare no competing financial interest.

ACKNOWLEDGMENTS

The authors gratefully acknowledge financial support by National Basic Research Program of China (973,

2012CB932800), Program for New Century Excellent Talents in University (MOE), Independent Innovation Foundation of Shandong University (2010JQ015), and National Natural Science Foundation of China (50971079).

REFERENCES

(1) Kelle, F.; Hunter, M. S.; Robinson, D. L. *J. Electrochem. Soc.* **1953**, *100*, 411−419.
(2) Thompson, G. E.; Furneaux, R. C.; Wood, G. C.; Richardson, J. A.; Gode, J. S. *Nature* **1978**, *272*, 433−435.
(3) Masuda, H.; Fukuda, K. *Science* **1995**, *268*, 1466−1468.
(4) Tsuchiya, H.; Macak, J. M.; Sieber, I.; Schmuki, P. *Small* **2005**, *7*, 722−725.
(5) Zwilling, V.; Aucouturier, M.; Darque-Ceretti, E. *Electrochim. Acta* **1999**, *44*, 921−929.
(6) Macak, J. M.; Tsuchiya, H.; Taveira, L.; Aldabergerova, S.; Schmuki, P. *Angew. Chem., Int. Ed.* **2005**, *44*, 7463−7465.
(7) Tsuchiya, H.; Schmuki, P. *Electrochem. Commun.* **2005**, *7*, 49−52.
(8) Tsuchiya, H.; Macak, J. M.; Sieber, I.; Taveira, L.; Ghicov, A.; Sirotna, K.; Schmuki, P. *Electrochem. Commun.* **2005**, *7*, 295−298.
(9) Sieber, I.; Kannan, B.; Schmuki, P. *Electrochem. Solid-State Lett.* **2005**, *8*, J10−J13.
(10) Sieber, I.; Hildebrand, H.; Friedrich, A.; Schmuki, P. *Electrochem. Commun.* **2005**, *7*, 97−100.
(11) Nishio, K.; Masuda, H. *Angew. Chem., Int. Ed.* **2011**, *50*, 1603−1645.
(12) Kinoshita, E.; Ingman, F.; Edwall, G.; Glab, S. *Electrochim. Acta* **1986**, *31*, 29−38.
(13) Llopis, J. F.; Gamboa, J. M.; Victori, L. *Electrochim. Acta* **1972**, *17*, 2225−2230.
(14) Burke, L. D.; Roche, M. B. C. *J. Electroanal. Chem.* **1985**, *186*, 139−154.
(15) Sun, J. Z.; Wang, Y. Z.; Zhang, C.; Kou, T. Y.; Zhang, Z. H. *Electrochem. Commun.* **2012**, *21*, 42−45.
(16) Trasatti, S.; Petrii, O. A. *Pure Appl. Chem.* **1991**, *63*, 711−734.
(17) Conway, B. E. *Prog. Surf. Sci.* **1995**, *49*, 331−452.
(18) Trasatti, S.; Petrii, O. A. *J. Electroanal. Chem.* **1992**, *327*, 353−376.
(19) Chierchie, T.; Mayer, C.; Lorenz, W. J. *J. Electroanal. Chem.* **1982**, *135*, 211−220.
(20) Horkans, J. *J. Electraanal. Chem.* **1986**, *209*, 371−376.
(21) Correia, A. N.; Mascaro, L. H.; Machado, S. A. S.; Avaca, L. A. *Electrochim. Acta* **1997**, *42*, 493−495.
(22) Jüttner, K.; Lorenz, W. J. *Z. Phys. Chem. N. F.* **1980**, *122*, 163−185.
(23) Qian, S. Y.; Conway, B. E.; Jerkiewicz, G. *Int. J. Hydrogen Energy* **2000**, *25*, 539−550.
(24) Jerkiewicz, G. *Prog. Surf. Sci.* **1998**, *57*, 137−186.
(25) Zhang, J. T.; Huang, M. H.; Ma, H. Y.; Tian, F.; Pan, W.; Chen, S. H. *Electrochem. Commun.* **2007**, *9*, 1298−1304.
(26) Pan, W.; Zhang, X. K.; Ma, H. Y.; Zhang, J. T. *J. Phys. Chem. C* **2008**, *112*, 2456−2461.
(27) Wang, X. G.; Wang, W. M.; Qi, Z.; Zhao, C. C.; Ji, H.; Zhang, Z. H. *Electrochem. Commun.* **2009**, *11*, 1896−1899.
(28) Dall'Antonia, L. H.; Tremiliosi-Filho, G.; Jerkiewicz, G. *J. Electroanal. Chem.* **2001**, *502*, 72−81.
(29) Grdeń, M.; Łukaszewski, M.; Jerkiewicz, G.; Czerwiński, A. *Electrochim. Acta* **2008**, *53*, 7583−7598.
(30) Hoare, J. P. *J. Electrochim. Soc.* **1964**, *111*, 610−615.
(31) Bagotzky, V. S.; Tarasevich., M. R. *J. Electroanal. Chem.* **1979**, *101*, 1−17.
(32) Seo, M.; Aomi, M. *J. Electrochem. Soc.* **1992**, *139*, 1087−1090.
(33) Hu, C. C.; Wen, T. C. *Electrochim. Acta* **1996**, *41*, 1505−1514.
(34) Tian, M.; Conway, B. E. *J. Electroanal. Chem.* **2005**, *581*, 176−189.
(35) Wagner, K.; Brankovic, S. R.; Dimitrov, N.; Sieradzki, K. *J. Electrochem. Soc.* **1997**, *144*, 3545−3555.
(36) Sieradzki, K.; Dimitrov, N.; Movrin, D.; McCall, C.; Vasiljevic, N.; Erlebacher, J. *J. Electrochem. Soc.* **2002**, *149*, B370−B377.
(37) Wenzel, R. N. *Ind. Eng. Chem.* **1936**, *28*, 988−994.
(38) Perdriel, C. L.; Custidiano, E.; Arvia, A. J. *J. Electroanal. Chem.* **1988**, *246*, 165−180.
(39) Bolzan, A.; Martins, M. E.; Arvia, A. J. *J. Electroanal. Chem.* **1986**, *207*, 279−292.
(40) Muller, L.; Maksimov, J. M.; Podlovchenko, B. I. *Elektrokhimiya* **1984**, *20*, 271−275.
(41) Rice, C.; Tong, Y.; Oldfield, E.; Wieckowski, A. *Electrochim. Acta* **1998**, *43*, 2825−2830.
(42) Arvia, A. J.; Salvarezza, R. C.; Triaca, W. E. *Electrochim. Acta* **1989**, *34*, 1057−1071.
(43) Kessler, T.; Visintin, A.; Bolzan, A. E.; Andreasen, G.; Salvarezza, R. C.; Triaca, W. E.; Arvia, A. J. *Langmuir* **1996**, *12*, 6587−6596.
(44) Tremiliosi-Filho, G.; Jerkiewicz, G.; Conway, B. E. *Langmuir* **1992**, *8*, 658−667.
(45) Gossner, K.; Mizera, E. *J. Electroanal. Chem.* **1981**, *125*, 347−358.
(46) Jerkiewicz, G. In *Interfacial Electrochemistry*; Wieckowski, A., Ed.; Elsevier: New York, 1999.
(47) Jerkiewicz, G.; Borodzinski, J. J. *Langmuir* **1993**, *9*, 2202−2209.
(48) Jerkiewicz, G.; Borodzinski, J. J. *J. Chem. Soc., Faraday Trans.* **1994**, *90*, 3669−3675.
(49) Cabrera, N.; Mott, N. F. *Rep. Prog. Phys.* **1948−1949**, *12*, 163−184.